Taylor & Francis
Taylor & Francis Group

Journal of Sustainable Forestry

ISSN: 1054-9811 (Print) 1540-756X (Online) Journal homepage: www.tandfonline.com/journals/wjsf20

Deep Transfer Learning for Predicting Microbial Attachment in Microbial Fuel Cells to Enhance Bioenergy Recovery

Mohammad Reza Chalak Qazani, Mostafa Ghasemi, Michael Seavers, Murtaza Ali Khan & Houshyar Asadi

To cite this article: Mohammad Reza Chalak Qazani, Mostafa Ghasemi, Michael Seavers, Murtaza Ali Khan & Houshyar Asadi (17 Mar 2026): Deep Transfer Learning for Predicting Microbial Attachment in Microbial Fuel Cells to Enhance Bioenergy Recovery, Journal of Sustainable Forestry, DOI: 10.1080/10549811.2026.2642663

To link to this article: https://doi.org/10.1080/10549811.2026.2642663

Published online: 17 Mar 2026.

JOURNAL OF SUSTAINABLE FORESTRY
https://doi.org/10.1080/10549811.2026.2642663

Taylor & Francis
Taylor & Francis Group

OPEN ACCESS Check for updates

Deep Transfer Learning for Predicting Microbial Attachment in Microbial Fuel Cells to Enhance Bioenergy Recovery

Mohammad Reza Chalak Qazani[a,b], Mostafa Ghasemi[c,d], Michael Seavers[e], Murtaza Ali Khan[b], and Houshyar Asadi[f]

[a]College of Science and Engineering, James Cook University, Townsville, Australia; [b]Faculty of Computing and Information Technology, Sohar University, Sohar, Oman; [c]Yangtze Delta Region Institute (Huzhou), University of Electronic Science and Technology of China, Huzhou, China; [d]Chemical Engineering Section, Faculty of Engineering, Sohar University, Sohar, Oman; [e]Department of Computer Science and Information Systems, Murray State University, Murray, KY, USA; [f]Institute for Intelligent Systems Research and Innovation (IISRI), Deakin University, Geelong, Australia

ABSTRACT
Microbial Fuel Cells (MFCs) offer a promising pathway for converting organic matter from biomass-rich wastewater into electricity while contributing to sustainable energy recovery. However, predicting and optimizing microbial attachment to electrodes – critical for power generation – remains a challenge. This study introduces a deep learning approach using transfer learning to predict microbial attachment patterns on electrode surfaces from scanning electron microscope (SEM) images. The methodology employs advanced convolutional neural networks (ResNet18 and VGG19_bn) that are fine-tuned on experimentally collected SEM images of MFC electrode surfaces. Among the tested models, ResNet18 achieved the highest accuracy (51.16%) in classifying microbial attachment levels, demonstrating the potential of AI-assisted bioenergy optimization. Findings confirm a positive correlation between microbial surface coverage and MFC performance, with higher attachment improving power density and COD removal efficiency. This research provides a framework for integrating artificial intelligence into bioenergy systems, supporting real-time monitoring and control of MFCs for efficient renewable energy generation.

KEYWORDS
Microbial fuel cell; biomass energy; transfer learning; sustainable forestry; deep learning for bioenergy; microbial attachment prediction

Introduction

With increasing population and global warming, societies face the challenge of developing sustainable energy systems from forest-based and biomass resources (Jacobson & Delucchi, 2011). As global industrialization continues, carbon dioxide emissions are expected to increase by more than 60% by 2030. Additionally, about half of the wastewater is discharged untreated (Zhou et al., 2019). Water scarcity and energy shortages are the world's biggest problems. The statistics show that around 66% of the world's population experiences water shortages for at least a month each year. Also, climate change and global warming (primarily due to fossil fuels and CO2) make this problem a crisis (Ghasemi et al., 2021). These challenges have prompted global strategies to utilize forestry residues and sustainable bioenergy pathways that minimize environmental impacts and enhance environmental benefits. That is why many scientists

CONTACT Mohammad Reza Chalak Qazani m.r.chalakqazani@gmail.com; mohamadreza.chalakqazani@jcu.au College of Science and Engineering, James Cook University, 1 James Cook Dr, Douglas, Townsville, QLD 4814, Australia

work on fuel cells that produce energy while releasing only water. Innovative technologies like microbial fuel cells (MFCs) have also been discussed in the context of biomedical and hazardous waste management, especially during crisis events such as the COVID-19 pandemic, highlighting their potential for sustainable bioremediation and circular energy solutions (Ojha et al., 2022). Further, Bose, Gopinath, et al. (2018) reviewed the use of MFCs for sustainable power generation from diverse wastewater sources, aligning well with broader circular bioeconomy and low-carbon forestry initiatives.

An MFC is a bio-electrochemical device capable of converting forest-derived biomass residues and forestry wastewater into renewable energy (Logan et al., 2006). The versatility of MFCs in converting diverse waste types into energy, including municipal and industrial wastewater, has been comprehensively reviewed by Ojha and Pradhan (2025). One of the key advantages of an MFC is that it can operate at high chemical oxygen demand (COD) and salinity, as well as at variable pH (Chen et al., 2022). MFC attracted more attention because it uses only wastewater as fuel and produces electricity as a clean fuel. So, MFC's main problem is the high capital price and low power generation (Logan & Regan, 2006). Electrochemical stimulation of microbial communities by Chlorella sp. metabolites has been shown to boost bioelectricity generation in MFCs by enhancing interspecific interactions and species diversity (Xu et al., 2019). Ancona et al. (2024) highlighted the dual potential of Plant MFCs (PMFCs) for bioelectricity generation and soil decontamination, emphasizing the importance of selecting appropriate plant species and electrode materials to optimize both energy production and pollutant remediation. Prathiba et al. (2024) highlight the importance of anode modification and the challenges of scaling up MFCs, focusing on enhancing power generation and optimizing electrode materials for commercial applications. Further insights into advancements in anode materials were provided by Satpathy et al. (2025), who reviewed recent modifications and performance evaluations, emphasizing improvements in surface chemistry and conductivity. Recent research by Bose et al. (2019) demonstrated that biomass-derived activated carbon significantly enhances cathode performance in MFCs, leading to sustainable power generation and lower material costs.

Sevda et al. (2023) investigated the effects of various factors, including electrode surface area, PEM area, and anodic chamber volume, on the performance of dual-chamber MFCs for wastewater treatment and electricity generation, highlighting the optimization of power density, wastewater treatment efficiency, and biofilm development. Similarly, Satpathy et al. (2022) have demonstrated the development of MFC-based dairy wastewater treatment systems, supporting the dual benefit of pollution mitigation and resource recovery. Han et al. (2023) demonstrated a synthetic three-species microbial alliance significantly enhancing MFC performance through synergistic interactions and substrate diversity. Kolubah et al. (2023) introduced a W2N-MXene composite anode catalyst in MFCs, significantly enhancing power density and wastewater treatment efficiency. The feasibility of using MFCs for simultaneous sewage treatment and bioelectricity generation has been experimentally validated by Bose, Dhawan, et al. (2018), underscoring the technology's dual environmental and energy benefits. Idris et al. (2023) explored palm kernel shell-derived modified electrodes, enhancing MFCs' power generation and formaldehyde bioremediation efficiency. You et al. (2023) present an innovative two-phase partitioning MFC that significantly improves propanetriol treatment efficiency and power generation.

Artificial intelligence (AI), including deep learning, has recently emerged as a powerful tool for bioenergy optimization in forestry systems, enabling predictive modeling and improved resource utilization (Yaman & Çalık, 2023). They have gained significant interest across Industry 4.0 (Rai et al., 2021). The machine learning-based models are designed and developed using the experimental datasets of the process. They are often more accurate than classical models. One of the pioneering studies on the application of machine learning to roll forming technology was conducted by Tardast et al. (2012). They studied the implementation of an artificial neural network (ANN) to accurately predict the performance of fabricated MFCs, demonstrating a strong correlation between actual and predicted data with minimal error. Pandya et al. (2024) emphasized the pivotal role of microbial communities in driving bioenergy generation in MFCs. They outlined microbial-electrode interactions as a key performance lever for future scalable systems. Recent reviews have highlighted the growing synergy between AI and MFCs, identifying key parameters that influence MFC efficiency and proposing data-driven control strategies to address nonlinearity and environmental variability (Ojha et al., 2025).

A study by Nazari (2012) demonstrated the effectiveness of gene expression programming in predicting the voltage output of PEM fuel cells, using a comprehensive dataset of 843 samples to train and test models, highlighting the potential of machine learning to forecast fuel cell performance under varying operational conditions accurately. The review paper by Recio-Garrido et al. (2016) explores advancements in bioelectrochemical systems, emphasizing the need for model-based optimization and control for commercialization. Monroy et al. (2018) developed and validated an ANN model to accurately predict biohydrogen production by photofermentation using an immobilized consortium of photobacteria, demonstrating its effectiveness across varying light conditions and its reliability and generalization capacity for both indoor and outdoor fermentations. Yewale et al. (2020) developed a temperature-based mathematical model for MFCs. They implemented a multi-model-based control strategy using machine learning, thereby improving controller performance. They found that the weighted k-nearest neighbor (WkNN) model switching criteria outperformed the various machine learning approaches. Vichard et al. (2020) used an Echo State ANN to model and predict the degradation of PEM fuel cells, demonstrating the effectiveness of AI-based approaches for forecasting performance loss and extending operational lifespan under variable conditions.

Shabani et al. (2021) developed an energy-autonomous water-quality sensing unit that utilizes an MFC for both sensory input and power generation, enabling accurate measurement of COD in natural pond water samples. Mowbray et al. (2021) provided a detailed survey of how machine learning (ML) can automate various aspects of bioprocess engineering, from predictive model building to experimental planning, emphasizing the potential and limitations of existing ML solutions in biotechnology and biopharma, and identifying key challenges and gaps that need to be addressed to integrate ML and AI tools effectively into bioprocess development. Liyanaarachchi et al. (2021) developed and applied an ANN model to accurately predict and optimize biomass and lipid production in Chlorella vulgaris, demonstrating superior predictive accuracy compared to traditional methods and identifying optimal cultivation conditions to maximize biodiesel production. Chou et al. (2022) developed an artificial intelligence model, specifically a deep convolutional neural network (CNN) optimized with a bio-inspired algorithm, for accurately forecasting the power generation capacity of plant MFCs based on environmental and device parameters. Wang et al. (2022) introduced a machine learning-assisted model to optimize PEM fuel cell parameters, significantly reducing nitrogen gas crossover and enhancing performance. Dwivedi et al. (2022) reviewed the integration of MFC technology with recent advances in nanotechnology, genetic engineering, additive manufacturing, artificial intelligence, and adaptive control, aiming to develop advanced, sustainable MFC systems to address the challenges of climate change and energy demand. Ta et al. (2022) developed an effective AI-based modeling and optimization tool for MEC-AD systems, demonstrating for the first time the application of a two-hidden-layer artificial neural network (ANN) and particle swarm optimization to significantly enhance biomethane recovery and waste treatment efficiency, providing valuable insights and decision-making support for the renewable energy and waste management sectors.

Recently, Sayed et al. (2024) used an ANN combined with a Forensic-Based Investigation (FBI) algorithm to optimize the performance of microalgae MFCs, significantly enhancing power density and COD removal by integrating ANN modeling with practical optimization techniques, despite challenges related to parameter tuning and performance validation. Rezk et al. (2023) developed a fuzzy modeling and equilibrium optimizer approach to determine optimal operating parameters for a ceramic-based MFC, resulting in a 5% increase in CMFC output power compared to experimental work and response surface methodology (RSM). (Lim et al. (2024) demonstrated the effectiveness of an ANN in predicting biofilm communities and power generation in MFCs from wastewater, with accuracies ranging from 62% to 92%, highlighting the potential of AI to replace complex metagenome analyses and address challenges in scale-up and parameter optimization, despite limitations in model refinement and application-specific adjustments.

A limited number of studies have investigated the impact of catalysts and PEMs on MFC performance (Han et al., 2023; Idris et al., 2023; Kolubah et al., 2023; Sevda et al., 2023; You et al., 2023). Also, the main focus of machine learning methods was the study of the influence of input parameters on MFC performance (Chou et al., 2022; Dwivedi et al., 2022; Lim et al., 2024; Liyanaarachchi et al., 2021; Monroy et al., 2018; Mowbray et al., 2021; Nazari, 2012; Recio-Garrido et al., 2016; Rezk et al., 2023; Sayed et al., 2024; Shabani et al., 2021; Ta et al., 2022; Tardast et al., 2012; Vichard et al., 2020; Wang et al., 2022; Yewale et al., 2020). This study aims to investigate, for the first time, the impact of bacterial attachment on electrode surfaces on the performance of MFCs in terms of COD removal and power generation. Previous research has paid limited attention to the relationship between bacterial attachment and MFC performance.

Various methods have been employed to quantify the extent of bacterial attachment to electrode surfaces, a fundamental concept involving the transfer of organic compounds and electrons to the electrodes. This research paper examines the correlation between the quantity of bacteria adhered to electrode surfaces and their impact on power generation and overall performance in MFCs. The attached microorganisms were detached from the surface and transferred to Petri dishes to determine the percentage of bacterial coverage on the electrode surface. Additionally, scanning electron microscopy (SEM) was employed for further visualization. There is a lack of extensive studies focusing on the attachment of microorganisms to electrode surfaces and the degree of surface coverage. Given the high operational costs of MFCs, particularly those associated with the cathode electrode and PEM, understanding microbial attachment to electrode surfaces can provide valuable insights into MFC operation and commercialization. This research is founded on the assumption that increased microbial adhesion on the electrode surface improves MFC efficiency by boosting power density, COD reduction, and coulombic efficiency. The extent of microbial adherence, as measured by SEM image analysis, is considered the primary factor affecting electrochemical activity and energy production efficiency.

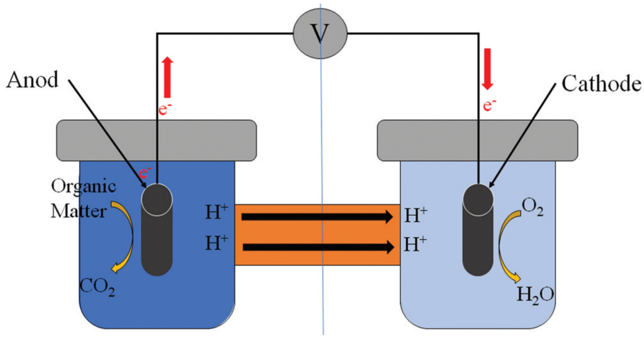

Figure 1. The schematic structure of an MFC.

The overview of the MFC, including the configuration, media, analysis/calculation, and microbial community, is explained in Section "Materials and methods". Section "Methodology" of the paper elaborates on the methodology, incorporating a pioneering approach of utilizing transfer and deep learning methods. Section "Results and discussions" of the paper presents the extracted results, which are carefully examined and discussed using Google Cloud's Vertex AI platform. Finally, Section "Conclusion" presents the conclusions drawn from the analysis.

Materials and methods

An MFC device uses microorganisms to convert organic matter into electrical energy. It harnesses bacteria's metabolic activity, enabling them to oxidize organic compounds and generate electrons that can be captured and used as a power source. MFCs have potential applications in wastewater treatment and renewable energy production. The schematic of the MFC is shown in Figure 1. In this Section, the MFC configuration, media, analysis/calculation, and microbial community are discussed.

MFC configuration

The MFC consisted of two chambers, an anode and a cathode, separated by Nafion 117 as the PEM. The PEM allows only protons to pass through, and the electrons pass through the external circuit to reach the anode (Jain, 2021). Carbon felt electrodes (Grade GFD, Sigma-Aldrich) with a projected surface area of 12 cm^2 served as both the anode and cathode. The cathode did not receive any more catalyst layers.

Then, electricity will be generated in the cathode chamber via the oxygen reduction reaction.

Media

The media in the anode chamber contained 5 g/L glucose, and 0.5 g/L yeast extract served as the nitrogen source. To improve the media, 10 mL of Wolf mineral solution per Liter of media, 4 g NaHCO3, and 0.2 g KCl were used. The media were then inoculated with anaerobic sludge from palm oil mill effluent (POME) plants. The cathode chamber consisted of 4.26 g/L Na_2PO_4, 2.5 g/L NaH_2PO_4, 0.13 g/L KCl, and 0.31 g/L NH_4Cl solution, while an aquarium pump performed aeration. A phosphate buffer solution has been utilized to adjust the pH (6.5–7) in the neutral condition. All chemicals were purchased from Sigma-Aldrich. The MFC was operated at ambient room temperature, and all experiments were performed in triplicate ($n = 3$); the average values were reported.

Analysis/calculation

For a known voltage, the current and power can be calculated by the formula as follows:

$$I = \frac{V}{R} \tag{1}$$

$$P = V \times I \tag{2}$$

where the current (ampere) is denoted by I, R is the symbol of external resistance (ohms), P is the produced power (watt) of the system, and V is the voltage (volt).

High-range COD reagents were used to measure COD (Chemical Oxygen Demand) accurately. To facilitate this process, collecting the sample from an anode chamber and diluting it by a factor of 10 is necessary. Next, a 2 ml portion of the diluted sample must be heated to 150°C, and the COD measurement should be taken using a spectrophotometer. Before measuring COD, the user should prepare a calibration curve. Additionally, a multimeter is used to measure the voltage. At the same time, the power is calculated by applying various loads to the system using Eqs. (1-2).

The coulombic efficiency (CE) was calculated as the ratio of the actual current over time to the maximum current achievable from the MFC. The CE was computed using the following formula:

$$CE = \frac{M \int_0^t I dt}{F b V_{an} \Delta \mathrm{COD}} \tag{3}$$

where $M = 32$ is the molecular weight of the oxygen molecule, and V_{an} is the volume of the anode occupied by the liquid and F is the Faraday constant.

The experimental setup included three separate MFC units (MFC1–MFC3) that were run under the same conditions, differing only in microbial attachment levels (7%, 12%, and 20%), which served as the independent variable. Every MFC chamber operated as a separate statistical unit, guaranteeing data independence and replicability. Every experimental condition was repeated three times to reduce measurement uncertainty. The dependent variables – power density, COD removal, and CE – were used to assess system performance at varying levels of microbial attachment.

Microbial community

In this study, we investigated microbial attachment on the electrode surface and its impact on MFC performance. To accurately assess microbial coverage, we employed a detailed image analysis approach that focuses on the area covered by microorganisms rather than simply counting their number. This methodology provides a direct correlation to MFC performance.

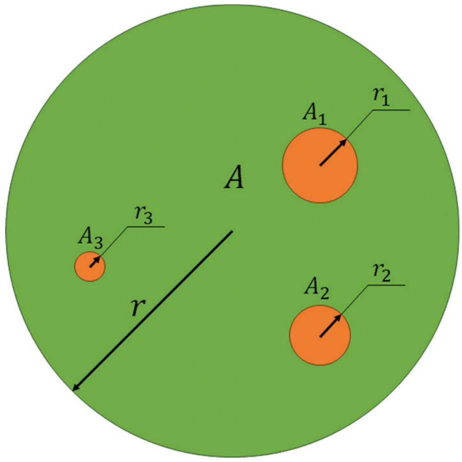

Figure 2. The surface of a Petri dish is covered with microorganism colonies.

Measurement of Microbial Coverage:

- Image Analysis Techniques: Microbial attachment was quantified by analyzing images of the colonies observed under a Petri dish. These images were captured using a scanning electron microscope (SEM) at a magnification of 5000X, utilizing the SE2 signal, which detects secondary electrons emitted from the sample. This signal is especially useful for visualizing the electrode's detailed surface morphology and for precise measurement of the area covered by microbial colonies.
- Quantification Method: To quantify microbial coverage, we used a grid-based method illustrated in Figure 2. This figure shows the process of overlaying a grid on SEM images and measuring the fraction of grid cells occupied by microorganisms.

The percentage of the surface which has been covered was found as follows:

$$\text{surface cover\%} = \frac{\sum_{i=1}^{n} A_i}{A} \tag{4}$$

where i is the colonies' number, and n is the number of colonies that are formed on the electrode.

Consideration of Exoelectrogen Colonization Methods:

- Diverse Colonization Strategies: Different species of exoelectrogens exhibit distinct colonization behaviors, including accumulation or dispersion. To address this variability, we categorized microorganisms according to their known colonization patterns. This categorization allows us to differentiate between species that form concentrated clusters and those that spread more evenly across the electrode surface.
- Implications for Data Interpretation: By considering these colonization strategies, we improved the accuracy of our data interpretation. For example, species with accumulation patterns might cover a larger area in specific regions. At the same time, those

with dispersion behaviors might show a more uniform distribution. This differentiation helps clarify the true impact of microbial coverage on MFC performance.

Impact on MFC Performance:

- Correlation with Power Generation: Assessing microbial coverage is vital for understanding its influence on MFC performance. As shown in our results, a higher percentage of electrode area covered by microorganisms generally correlates with enhanced power generation in MFCs. This is because a larger microbial biofilm provides a greater surface area for electrochemical reactions, thus improving the efficiency of electron transfer and electricity generation.

Methodology

The proposed methodology for this study is based on deep and transfer learning methods, which are the focus of this Section. Sub-images of the SEM are used in this study to capture the system output (the attachment number of microbes in the MFC) based on the system's input (the SEM sub-image). Then, the transfer learning method using the base CNN (including VGG19, Wide ResNet, VGG13, ResNet18, AlexNet, VGG19 with Decay, Wide ResNet with Decay, VGG13 with Decay, ResNet18 with Decay, and AlexNet with Decay as the base model) is used to extract the appropriate model using the limited database.

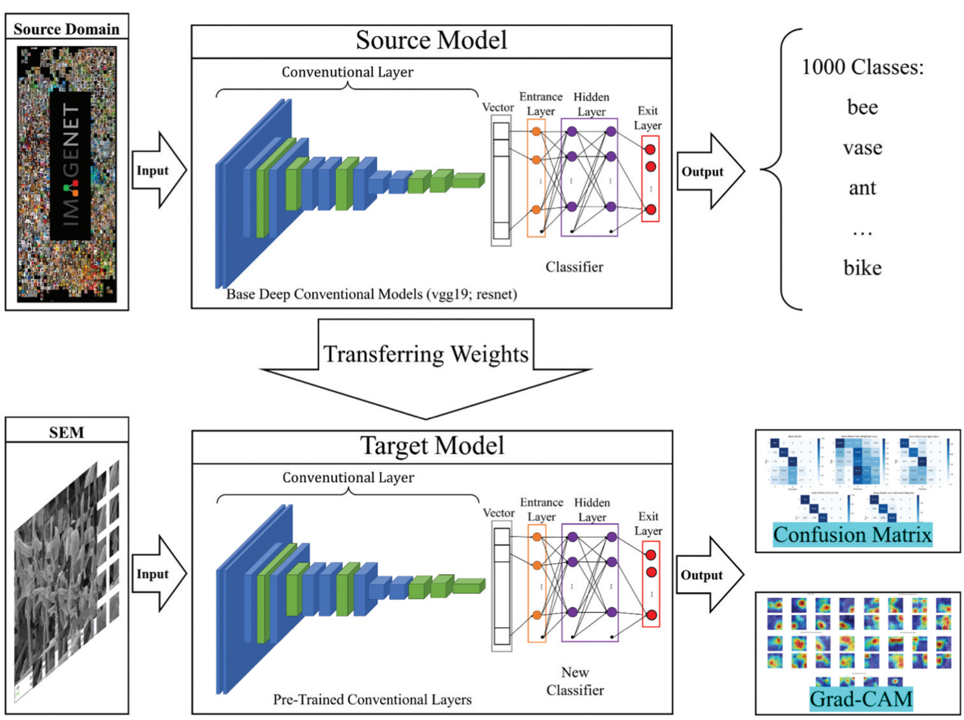

Figure 3. Block diagram of the proposed transfer learning-based model for the amount of microbes' attachment in membrane-less MFC.

Figure 3 illustrates the block diagram of our proposed transfer-learning-based model for quantifying microbial attachment in membrane-less MFCs. The core idea behind transfer learning involves leveraging two datasets that share similarities. These datasets are utilized to train both the source and target models. Transferring knowledge from the source model to the target model can accelerate training for the target task. In this study, we employ the fine-tuning approach to achieve satisfactory results. Our study employs transfer learning methods to predict microbial attachment. This phenomenon is challenging, and even impossible, to detect directly. Notably, no transfer-learning-based convolutional neural network has been previously used to diagnose microbe attachment issues. It should be emphasized that the raw datasets cannot be directly fed into the algorithm without compromising the model's accuracy. Hence, we discuss data preprocessing as the first subsection in this section before explaining our proposed transfer learning model. Subsequently, we present the transfer learning-based model used to predict microbe attachment in the following section.

Preprocessing

Field-emission scanning electron microscopy (FESEM, SUPRA 55 VP, Zeiss, Germany) was used to observe the morphology and attachment of microorganisms on the electrode surface. The SEM analysis was conducted without an evaporation coating; however, for clearer images, samples typically need to be coated with gold or another conducting metal. The microorganisms were observed at 5 KX magnification, and the signal was SE2. It should be noted that the SE2 signal in scanning electron microscopy (SEM) refers to the secondary electron signal collected by a detector, providing detailed surface imaging and topographical information of the sample at high magnification. We captured three SEM images for each excipient, producing six original SEM images. The original images are in RGB format with a resolution of 1027×768 pixels, a density of 146 dpi and a depth of 24 bits. The images were resized to sub-images with a resolution of 1225×875 pixels to facilitate analysis.

We divided six original SEM images for each excipient into training, validation, and test sets. Each original SEM image had dimensions of 1225×875 pixels, and we sequentially divided them into 35 sub-images (7 sub-images in the raw and 5 sub-images in the column), each measuring 175×175 pixels. These sub-images are shown inside the supplementary file. Consequently, the training, validation, and test sets consisted of 120, 45, and 45 sub-images. To reduce overfitting due to the small sample size and improve generalization, we applied data augmentation techniques – rotation, horizontal flipping, and scaling – to the dataset. This increased the variability of training data and better simulated real-world conditions observed in SEM images. This decision was made to preserve the authenticity of the features extracted from the training dataset by maintaining the integrity of the original images.

To move beyond simple descriptive statistics, this study employs a hypothesis-driven and inferential approach. Each of the three independent MFC units was assigned to each level of attachment ($n = 3$; total $N = 9$), with each reactor operating as a distinct statistical unit to guarantee replication and independence. The level of microbial attachment was analyzed as a fixed factor. At the same time, biological parameters across replicates were treated as random error terms, enabling proper statistical analysis. Since the SEM image dataset serves as a case study, only applicable case-specific model evaluation techniques – 5-fold cross-validation, external test data, and performance metrics – were utilized, rather than relying solely on descriptive summaries.

Transfer learning

Transfer learning is a proposed solution for addressing learning challenges across different domains. When deep learning is combined with transfer learning, it leads to significant enhancements in the accuracy and precision of fault diagnosis methods. The process of transfer learning involves two key steps. First, a source neural network is trained on a specific dataset and task. Then, the learned features and knowledge are transferred to a new network, aiding the training process for a related target dataset.

Transfer learning involves two distinct domains: a source domain $D_s = \{\mathcal{X}_s, P_s(x_s)\}$ and a target domain $D_t = \{\mathcal{X}_t, P_t(x_t)\}$. The feature spaces of the source and target domains are denoted as $\mathcal{X}_s$ and $\mathcal{X}_t$, respectively. Additionally, $P_s(x_s)$ and $P_t(x_t)$ represent the respective marginal probability distributions associated with each domain.

Transfer learning aims to enhance the performance of the target predictive function $f_t(.)$ in the target domain D_t by leveraging knowledge acquired from a different source domain D_s and its associated learning task T_s, under the condition that D_s is not equal to D_t and T_s is not equal to T_t. When $T_s \neq T_t$, a prevalent subproblem in transfer learning arises, known as domain adaptation.

Transfer learning facilitates the transfer of learned features across various learning tasks. It primarily focuses on enhancing the training phase of deep learning by enabling effective feature extraction and transfer across multiple datasets with similar problem characteristics. Transfer learning involves utilizing pre-trained layers from a source task to address a target task. A pre-trained model with its fully connected layers removed is employed. In contrast, its convolutional and pooling layers are frozen (their weights remain unchanged) to serve as feature extractors. The weights of the fully connected layers (classifier section) need to be updated to adapt the pre-trained network to the target dataset and optimize target classification. Transfer learning encompasses two distinct approaches: feature extraction and fine-tuning. In the feature extraction approach, the fully connected layers are entirely replaced. New fully connected layers are integrated with the frozen pre-trained layers based on the target dataset. Conversely, during fine-tuning, the fully connected layers of the pre-trained model are retained, with only their weights updated.

Objective function

To evaluate the classification performance of the model, a confusion matrix was used to count true positives (TP), false negatives (FN), false positives (FP), and true negatives (TN). Subsequently, performance measures such as accuracy, precision, recall, and F-measure were calculated from the confusion matrix. The following equations define the calculation of these measures (Fawcett, 2006).

$$Accuracy = \frac{TP + TN}{TP + FP + TN + FN} \tag{5}$$

$$Precision = \frac{TP}{TP + FP} \quad (6)$$

$$Recall = \frac{TP}{TP + FN} \quad (7)$$

$$F - measure = 2 \times \frac{Precision \times Recall}{Precision + Recall} \quad (8)$$

Across the five experiments presented earlier in this section, several parameters were kept constant. First, all models were trained for 20 epochs, with model checkpoints saved at the epoch with the highest validation accuracy. Second, all models were trained using stochastic gradient descent (SGD) with a momentum of 0.9. A cosine annealing learning rate scheduler was also applied, reducing the learning rate to 1% of the initial value over all 20 epochs. Third, all models were trained on a GPU, and our SpinalNet layer used a width of 125. Lastly, to ensure reproducibility across multiple runs, all models were run with CUDA deterministic enabled, and a seed (42) was set across all libraries.

The six SEM images were divided into sub-images and subsequently allocated to the training, validation, and test sets, comprising 120, 45, and 45 SEM sub-images, respectively. It is important to note that careful consideration was given to ensure that the captured areas of the six SEM images did not overlap. As a result, the test set served as external validation data to assess the accuracy of predictions for unfamiliar images that were not utilized during the training and validation stages. Moreover, five distinct datasets were created to explore different combinations of SEM images. The CNN model was constructed iteratively using these datasets, and classification accuracy on the test set was assessed in five replicate cycles. Finally, the average value of each statistical index was calculated. Results and Discussions

Results and discussions

This section presents the results of running MFC and the proposed transfer learning-based CNN against each of the pre-trained models. Models were run on Google Cloud using its Vertex AI platform. The virtual machine (VM) used runs Debian 11. The VM uses four 2-core vCPUs, 16 GB of memory, and a single NVIDIA T4 vGPU with 16 GB of memory. Additionally, the VM runs on the TensorFlow Enterprise 2.11 (Intel® MKL-DNN/MKL) environment.

MFC performance

Figure 4(a) shows the power density curve of some MFCs with different attachment of microorganism MFC1 (7% attachment of microorganisms on the electrode's surface), MFC2 (12%) and MFC3 (20%). Also, MFC1, which has 7% attachment of microorganisms to the electrode surface, produced the lowest power density of 145 mW/m2. MFC2, with 12% attachment, produced 188 mW/m2, and MFC3, with 20% attachment, produced 193.4 mW/m2, the highest power output. The CE and COD removal of the MFCs was shown in Figure 4(b). As shown, MFC2 and MFC3 have almost identical COD removal of about 73%. MFC3, with greater microorganism attachment to the electrode surface, has a higher CE

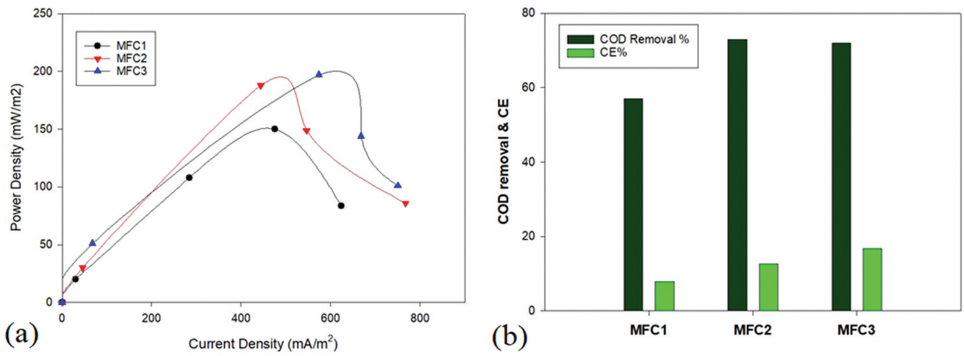

Figure 4. (a): Power density; (b): COD removal & CE of the MFCs.

(18.5%) than MFC2 (11.8%). MFC1 could also reduce the COD by 57% and has the lowest CE at about 5.6%.

ResNet training parameters

As mentioned in the previous section, we conducted five experiments using transfer-based learning models to evaluate their performance and limitations on our dataset. Resnet18 was selected as our main base model due to its suitability for small datasets and its competitive performance in our limited experiments. To select training parameters, we ran a test with three batch sizes (16, 32, and 64) and three learning rates (1 × 10^-2, 1 × 10^-3, and 1 × 10^-4). Table 1 reports the mean test accuracy and corresponding standard deviation for each combination of batch size and learning rate. Across all combinations, the best-performing parameters were a batch size of 16 or 32 and a learning rate of 1 × 10^-2, achieving a mean accuracy of 68.57% ± 1.99 SD. As the batch size and learning rate increased, accuracy decreased, with a larger SD. Due to our limited dataset, our base model tended to favor a high learning rate and a small batch size. For the remaining experiments in this section, all models will use a batch size of 16 (selected arbitrarily from the two best-performing sizes) and a learning rate of $1 \times 10 - 2$.

To understand the accuracy per class, we generated a confusion matrix for the selected model. Figure 5 illustrates the model's matrix as a percentage calculated across all five folds. From that matrix, along with the other high-performing models described in Table 1, we found that classification 0–2 had near-perfect predictions. In contrast, classifications 3 and 4 had accuracies approaching 0%. In all models, we found that class 4 was massively

Table 1. Mean test accuracy (± SD) for each batch × learning rate combination. The best result is shown in bold.

	Learning Rate		
Batch Size	1 × 10 − 2	1 × 10 − 3	1 × 10 − 4
16	68.57 ± 1.99	66.19 ± 4.26	42.86 ± 5.58
32	68.57 ± 1.99	65.71 ± 2.13	37.62 ± 5.43
64	66.19 ± 4.58	59.05 ± 4.26	24.29 ± 5.68

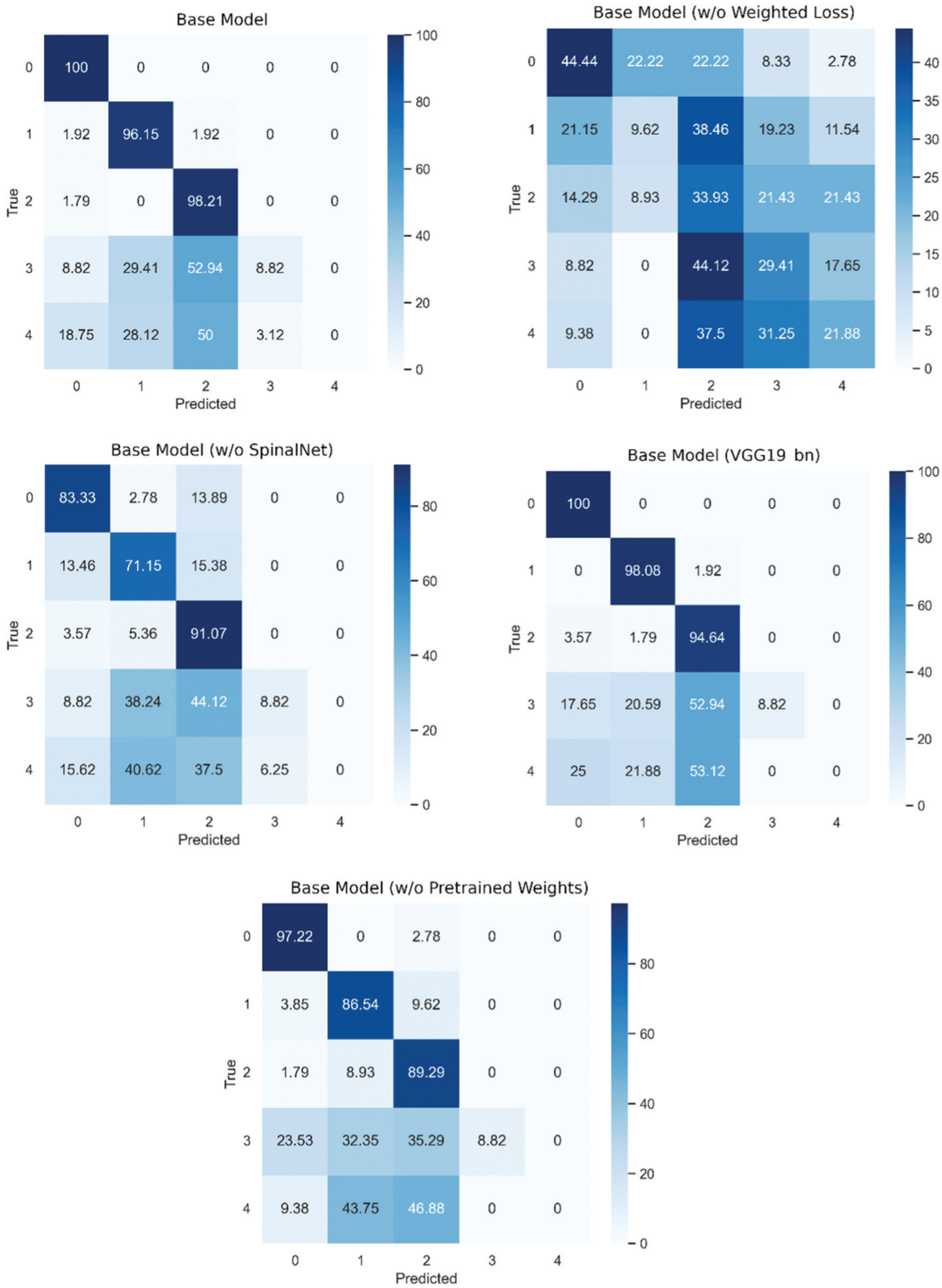

Figure 5. Confusion matrices of all models (values in %).

misclassified. These misclassifications indicate that either the models are overfitting or the data from other classes is too similar.

We can further analyze the problem by isolating it using Gradient-weighted Class Activation Mapping (Grad-CAM). By extracting the gradient from the last convolutional

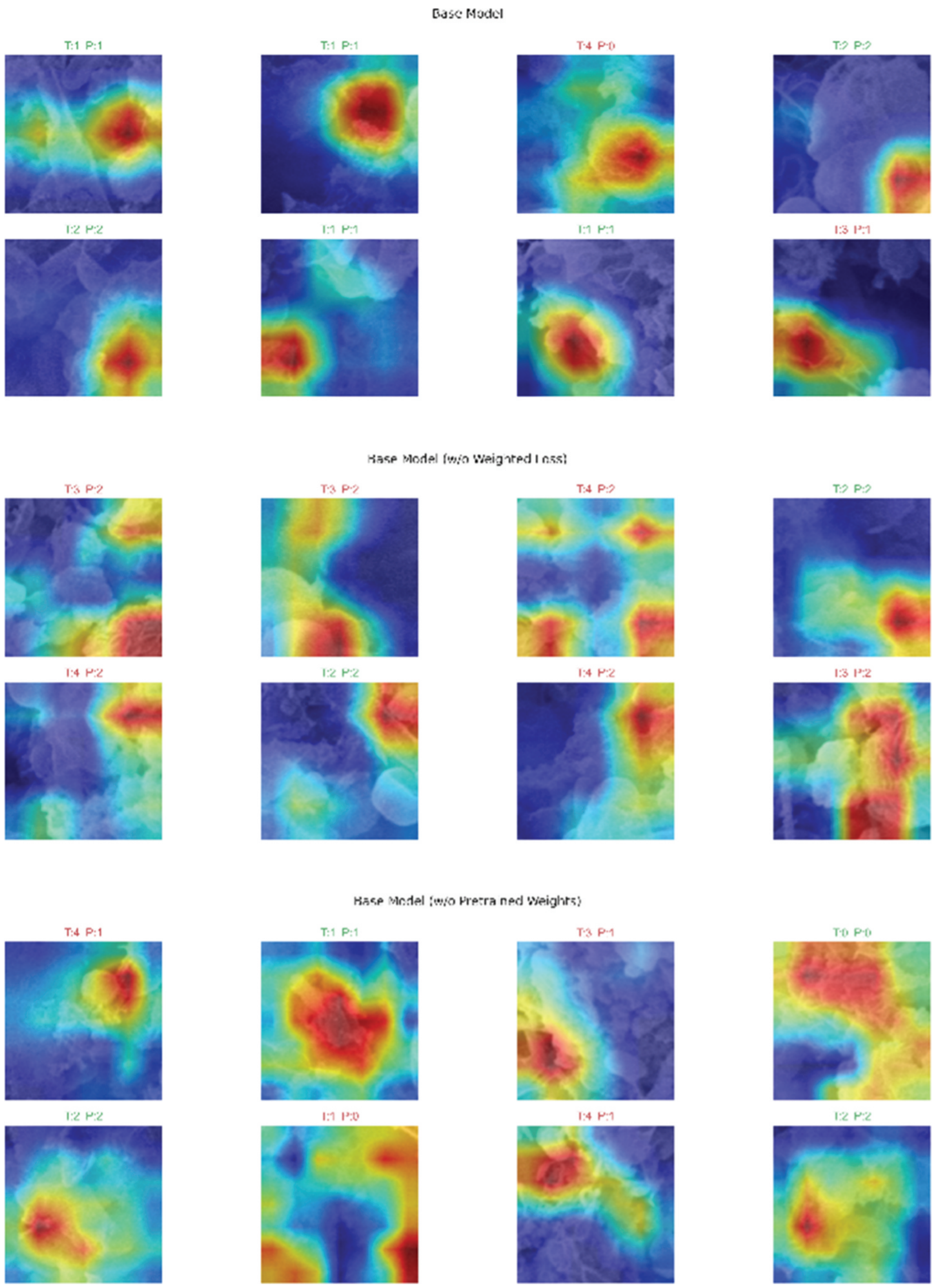

Figure 6. Grad-CAMs of best Fold from all Models.

layer and combining it with the feature map, we can identify which parts of the image contribute to the model's predictions. Figure 6 shows the Grad-CAMs (eight randomly selected images from the test split) for our best-performing model in the best-performing

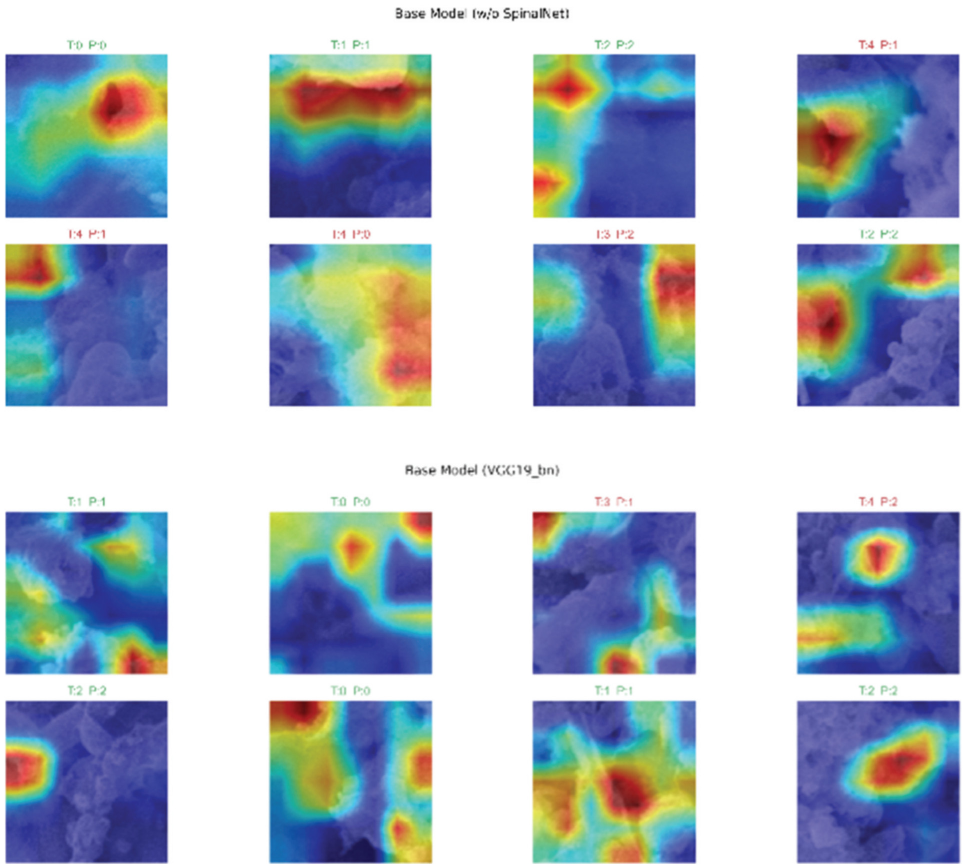

Figure 6. (Continued).

fold. Most of the image is irrelevant to the model, while the focused area highlights the microorganism's edges.

One misclassified class is shown, predicted as class 1 but labeled as class 3. By viewing the other maps of the correct class, we can see that the model is using the dark (black) areas in its predictions, which explains why it predicted class 1, as the other images of this class have this dark area. We can also use the training and validation accuracy and loss over all epochs to understand the models. Figure 7 illustrates these trends over the whole 20 epochs. The data was average across all five folds, with the shaded regions representing the standard deviation. Both accuracies increased over the epochs, following similar curve outlines. Likewise, the loss curve showed a similar trend, decreasing at each epoch. The validation split showed greater variability in both accuracy and loss, and its loss remained moderately above 1—a result we expected given our limited dataset. There may be slight overfitting, but overall, the model shows some stability.

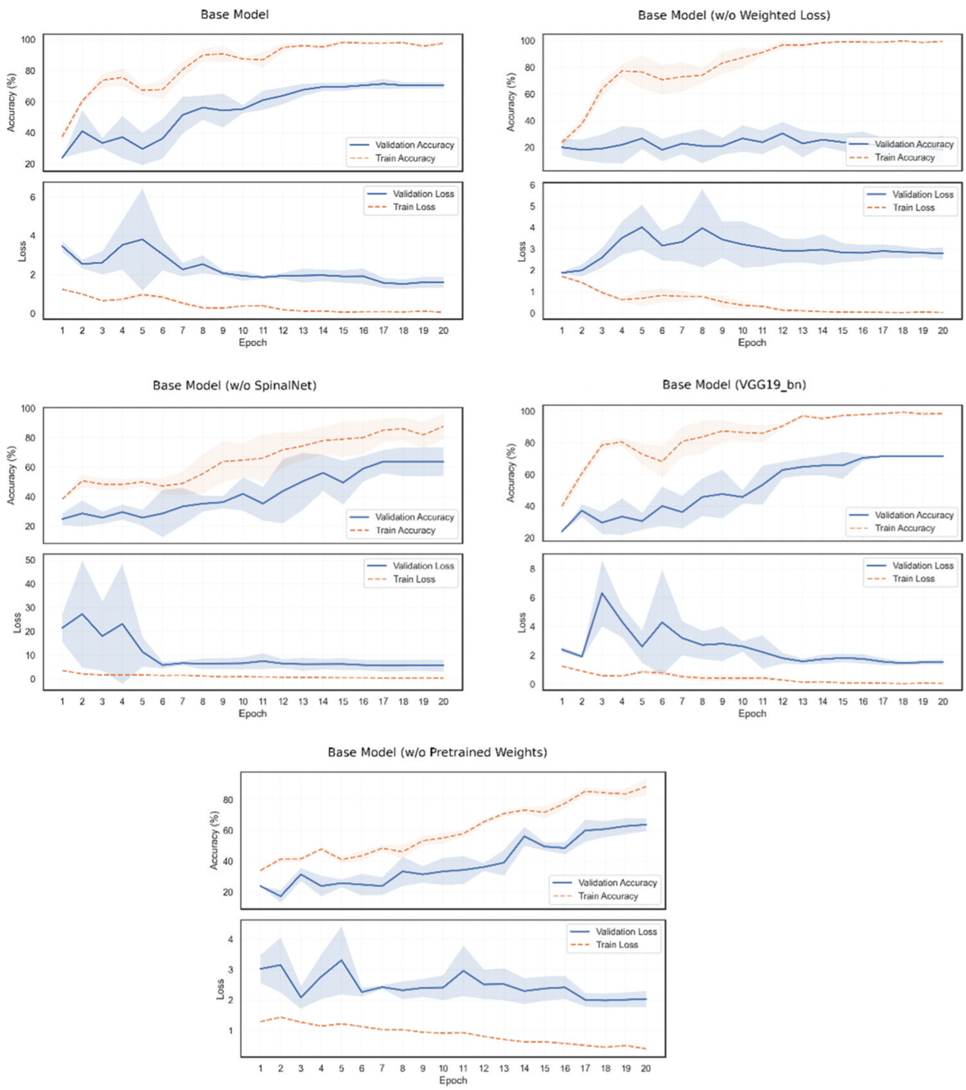

Figure 7. Cross-validation performance of all models.

Different models

ResNet without weighted loss

The sub-images in our dataset are not evenly distributed across all five classifications. The splits are composed of 36, 52, 56, 34, and 32 images, respectively. During testing, it was found that without a weighted loss, accuracy was extremely low, with moderate SD. Table 2 showcases the average test statistical indices across five folds of all experiments, including a test without weighted loss. The mean accuracy of this test is only slightly higher than random guessing (~23%) at 27.14% with a ± 5.98 SD.

Although the mean accuracy was low, this model achieved higher accuracy in classes 3 and 4, as shown in Figure 7. We observe that class 3 was the most misclassified, but the results are better than those of the base model. However,

Table 2. Average test statistical indices across five folds of all five experiments.

Experiments	Averages (%)	Precision	Recall	F1-Score
Base Model	Macro	52.9	60.6	52.1
	Weighted	56.6	68.6	58.2
	Test Mean	68.57 ± 1.99		
Without Loss	Macro	23.9	27.5	21.1
	Weighted	24.2	27.1	21.3
	Test Mean	27.14 ± 5.98		
Without SpinalNet	Macro	43	51	43.7
	Weighted	46.9	57.6	48.9
	Test Mean	57.62 ± 7.79		
Without Pretrained Weights	Macro	51.3	56.3	48.3
	Weighted	54.3	63.3	53.6
	Test Mean	63.33 ± 7.06		
VGG19_bn Base Model	Macro	54.43	60.3	51.7
	Weighted	58	68.1	57.8
	Test Mean	68.1 ± 2.71		

classes 0–2 show greater variability than in the base model, with class 1 still achieving the highest accuracy. In the Grad-CAMs (Figure 6), we can see larger predicted estimates, indicating more uncertainty in their predictions. Based on these estimates, we conclude that the model is unable to detect patterns or identify underlying classification differences. These results can be further examined in the cross-validation performance (Figure 7), where the training accuracy and loss are nearly identical to those of the base model. However, the validation split yields the worst results compared to the other models. The validation accuracy remained relatively constant, overall indicating that the model was overfitting. With the addition of the weighted loss, although some classes (3 and 4) decreased moderately, our model overall benefited by reducing overfitting and achieving higher accuracy on the top three classes, which contained the majority of sub-images.

ResNet without spinalNet

To ensure the addition of the SpinalNet layer was helping our models, we ran an experiment using solely Resnet19 on our dataset. As shown in Table 2, this model yielded moderate results (57.62%) but still achieved the second-best accuracy across all five tests. Additionally, this model yields the highest variance (±7.79). Although the accuracy and variance differ significantly from those of our base model, the confusion matrix (Figure 5) is similar to it. The top three classes (0–2) remain dominant, albeit on a smaller scale. Although there is more variance, class 4 is still never predicted, while class 3 is rarely predicted, even wrongly. The Grad-CAMs (Figure 6) cover larger areas than those of the previous models. In these maps, the model associates color (grayscale) with its learning, resulting in a focus on the darker shades and their amounts.

Additionally, the loss of validation is the highest (peaked at ~27 ± 20), even compared to the model without a weighted loss. The accuracy, on the other hand, increases steadily. However, as the validation loss stalls at epoch six, the model's confidence in predicting is poor, especially compared to the base model. This model also stalled at the earliest epoch, 6, again demonstrating its inability to make predictions confidently. Overall, with the addition of SpinalNet, our models' confidence improved, and their generalization improved.

ResNet without Pretrained Weights

As our primary goal is to examine transfer learning, we also employed a non-transfer learning model for comparison with our base model. This model still utilized the SpinalNet layer, but we trained it from scratch on our dataset. As a result, we found better results (63.33% – Table 2) than without SpinalNet and Weighted Loss; however, our base model still exceeded the accuracy. In addition, similar to the model without SpinalNet, the SD was the second highest at ±7.06. Figure 5 shows the confusion matrix, which is an improvement over the last few models, but slightly less accurate than the base model. The Grad-CAMs have the largest areas across all the models, again generalizing to the image colors. The cross-validation performance (Figure 7) is similar to that of the base model, but with a smoother training accuracy and loss curve. The SD of the validation line is also higher, with later epochs exhibiting greater variance than in the base model. Overall, without the pretrained weights in the ResNet model, we still get relatively high results. However, by starting with a pre-trained model, we achieve higher accuracy and greater stability.

VGG19_bn Base Model

Aside from ResNet19, we selected another base model for comparison with our original model. We chose VGG19_bn as the model due to its compatibility with small and/or limited datasets, such as ours. As shown in Table 2, this model performed second-best, with a mean accuracy of 68.1% and a low SD of ±2.71. The confusion matrix of this model is almost identical to the base model; classes 2 and 3 are swapped. Similarly, the cross-validation performance is almost identical, except that the validation curve in the base model is smoother and less spiky in the loss. Lastly, the Grad-CAMs show more exploration compared to the base model. Overall, although our base model performed best across all experiments, the best-performing models also utilized transfer learning.

Significance, limitations, and outlook

This study addresses a key challenge in the development of sustainable forestry systems – efficient bioenergy generation from biomass-derived wastewater. By employing deep transfer learning techniques to predict microbial attachment levels in MFCs, we introduce an image-based framework that directly supports low-carbon forestry practices. The approach aligns with sustainable forestry goals by enabling real-time monitoring and optimization of MFCs treating forestry and agro-industrial wastewater.

The novelty of this work lies in integrating CNN-based microbial surface analysis with experimental bioelectrochemical performance data, which, to the best of our knowledge, has not been previously explored in the context of forestry-related MFC systems. Unlike previous AI applications that focused solely on electrical output or chemical input variables, our model captures spatial microbial dynamics on electrode surfaces, offering a new dimension to bioenergy prediction and control.

We acknowledge that the study has certain limitations. The primary constraint is the limited number of original SEM images, which can limit model generalizability. However, we have addressed this through data augmentation, 5-fold cross-validation, class balancing with weighted loss functions, and Grad-CAM-based visualization to improve interpretability and reduce overfitting. These strategies strengthen the robustness of our findings within the constraints of limited data.

Although this research effectively showcases the potential of deep transfer learning for predicting microbial attachment and its relationship with MFC performance, we recognize a limitation in the substrate used for validation. The experiments were carried out with a synthetic medium containing glucose and an inoculum sourced from palm oil mill effluent (POME). To align directly with the sustainable forestry emphasis of this study, subsequent efforts will verify the proposed AI model using real lignocellulosic wastewaters, including those from pulp, paper, and wood-processing sectors. These substrates comprise intricate polymers, such as cellulose, hemicellulose, and lignin, that pose distinct challenges for microbial breakdown and electron transfer. Demonstrating the model's precision using these forestry residues would be an essential step toward its implementation in decentralized, forest-decentralized, and forestovery systems. The broader implications of this study extend to the automation and intelligent control of MFCs for renewable energy generation. The methodology proposed here provides a foundation for deploying AI-powered systems in decentralized forestry operations, particularly in remote areas with limited access to laboratory facilities. This supports scalable, sustainable energy recovery solutions aligned with circular-economy principles in the forestry sector.

Aside from ResNet19, we selected another base model for comparison with our original model. We chose VGG19_bn as the model due to its compatibility with small and/or limited datasets, such as ours. As shown in Table 2, this model performed second-best, with a mean accuracy of 68.1% and a low SD of ±2.71. The confusion matrix of this model is almost identical to the base model; classes 2 and 3 are swapped. Similarly, the cross-validation performance is almost identical, except that the validation curve in the base model is smoother and less spiky in the loss. Lastly, the Grad-CAMs show more exploration compared to the base model. Overall, although our base model performed best across all experiments, the best-performing models also utilized transfer learning.

Conclusion

In this paper, we presented the impact of microorganism attachment on microbial fuel cell (MFCs) performance by analyzing colonies observed under a Petri dish. The dataset was classified based on the electrode's covered area and Scanning Electron Microscope (SEM) data. Two transfer learning methods, namely VGG19_bn and ResNet18, based on SEM sections, were utilized to predict the attachment amount, a crucial factor for power generation in MFCs. Additionally, three other experiments were conducted to examine the effectiveness of transfer learning models compared to traditional models. The analysis involved creating confusion matrices averaged across the 5-fold cross-validation of each model across all five experiments, yielding two main observations.

First, across all experiments except the model without weighted loss, there was a significant bias toward the top three classes (0–2), with class 4 being neither predicted correctly nor incorrectly. Secondly, without using a weighted loss, due to our class imbalance, our model showed significant overfitting, with a bias toward class 2. Four statistical indices were calculated: classification accuracy, precision, recall, and F-measure. Each model's accuracy exceeded its precision, with ResNet-18 serving as our base model and achieving the highest accuracy. The recall of each model was slightly higher than its precision, indicating that our models are better at finding positive cases but include a few false positives. Although our models are not fully accurate, the study focused on identifying models with an accuracy of around 70%. Most models achieved above 60% with our main models reaching close to 70%. The ResNet18 transfer learning method demonstrated the highest efficiency with an accuracy of 68.57%.

In conclusion, the research successfully explored the impact of microorganism attachment on MFC performance using image analysis techniques and transfer learning methods. The findings highlighted overfitting in specific models and the importance of accuracy in predicting attachment levels. The ResNet18 transfer learning method proved most efficient in this study, providing valuable insights for enhancing MFC performance and wastewater treatment processes.

Disclosure statement

No potential conflict of interest was reported by the author(s).

Data availability statement

Data will be available upon request from the corresponding author.

References

Ancona, V., Cavone, C., Grenni, P., Gagliardi, G., Cosentini, C., Borello, D., & Barra Caracciolo, A. (2024). Plant microbial fuel cells for recovering contaminated environments. *International Journal of Hydrogen Energy*, *72*, 1116–1126. https://doi.org/10.1016/j.ijhydene.2024.05.457

Bose, D., Dhawan, H., Kandpal, V., Vijay, P., & Gopinath, M. (2018). Bioelectricity generation from sewage and wastewater treatment using two-chambered microbial fuel cell. *International Journal of Energy Research*, *42*(14), 4335–4344. https://doi.org/10.1002/er.4172

Bose, D., Gopinath, M., & Vijay, P. (2018). Sustainable power generation from wastewater sources using microbial fuel cell. *Biofuels, Bioproducts and Biorefining*, *12*(4), 559–576. https://doi.org/10.1002/bbb.1892

Bose, D., Sridharan, S., Dhawan, H., Vijay, P., & Gopinath, M. (2019). Biomass derived activated carbon cathode performance for sustainable power generation from microbial fuel cells. *Fuel*, *236*, 325–337. https://doi.org/10.1016/j.fuel.2018.09.002

Chen, J., Yang, J., Wang, R., Yang, Y., & Liu, Y. (2022). Design and research progress of nano materials in cathode catalysts of microbial fuel cells: A review. *International Journal of Hydrogen Energy*, *47*(41), 18098–18108. https://doi.org/10.1016/j.ijhydene.2022.04.020

Chou, J. S., Cheng, T. C., Liu, C. Y., Guan, C. Y., & Yu, C. P. (2022). Metaheuristics-optimized deep learning to predict generation of sustainable energy from rooftop plant microbial fuel cells. *International Journal of Energy Research*, *46*(15), 21001–21027. https://doi.org/10.1002/er.8538

Dwivedi, K. A., Huang, S.-J., & Wang, C.-T. (2022). Integration of various technology-based approaches for enhancing the performance of microbial fuel cell technology: A review. *Chemosphere*, *287*, 132248. https://doi.org/10.1016/j.chemosphere.2021.132248

Fawcett, T. (2006). An introduction to ROC analysis. *Pattern Recognition Letters*, *27*(8), 861–874. https://doi.org/10.1016/j.patrec.2005.10.010

Ghasemi, M., Nassef, A. M., Al-Dhaifallah, M., & Rezk, H. (2021). Performance improvement of microbial fuel cell through artificial intelligence. *International Journal of Energy Research*, *45*(1), 342–354. https://doi.org/10.1002/er.5484

Han, J.-Y., Zhang, H.-L., Guo, H., Liu, A.-Q., Nawab, S., Liu, N., Hui, M., Zhai, D.-D., & Yong, Y.-C. (2023). A rational designed synthetic three-species alliance system for synergetic improvement on power generation from microbial fuel cell. *Chemical Engineering Journal*, *481*, 148366. https://doi.org/10.1016/j.cej.2023.148366

Idris, M. O., Ibrahim, M. N. M., Noh, N. A. M., Yaqoob, A. A., & Hussin, M. H. (2023). Synthesis and fabrication of palm kernel shell-derived modified electrodes: A practical step towards the industrialization of microbial fuel cells. *Chemical Engineering Journal*, *475*, 146321. https://doi.org/10.1016/j.cej.2023.146321

Jacobson, M. Z., & Delucchi, M. A. (2011). Providing all global energy with wind, water, and solar power, part I: Technologies, energy resources, quantities and areas of infrastructure, and materials. *Energy Policy*, *39*(3), 1154–1169. https://doi.org/10.1016/j.enpol.2010.11.040

Jain, M. V. (2021). Production of electricity with the help of MFC cell. *Int Res J of Eng Technol (IRJET)*, *8*(4), 53–55.

Kolubah, P. D., Mohamed, H. O., Ayach, M., Rao Hari, A., Alshareef, H. N., Saikaly, P., Chae, K.-J., & Castaño, P. (2023). W2N-MXene composite anode catalyst for efficient microbial fuel cells using domestic wastewater. *Chemical Engineering Journal*, *461*, 141821. https://doi.org/10.1016/j.cej.2023.141821

Lim, C. E., Chew, C. L., Pan, G.-T., Chong, S., Arumugasamy, S. K., Lim, J. W., Al-Kahtani, A. A., Ng, H.-S., & Abdurrahman, M. (2024). Predicting microbial fuel cell biofilm communities and power generation from wastewaters with artificial neural network. *International Journal of Hydrogen Energy*, *52*, 1052–1064. https://doi.org/10.1016/j.ijhydene.2023.08.290

Liyanaarachchi, V. C., Nishshanka, G. K. S. H., Sakarika, M., Nimarshana, P., Ariyadasa, T. U., & Kornaros, M. (2021). Artificial neural network (ANN) approach to optimize cultivation conditions of microalga Chlorella vulgaris in view of biodiesel production. *Biochemical Engineering Journal*, *173*, 108072. https://doi.org/10.1016/j.bej.2021.108072

Logan, B. E., Hamelers, B., Rozendal, R., Schröder, U., Keller, J., Freguia, S., Aelterman, P., Verstraete, W., & Rabaey, K. (2006). Microbial fuel cells: Methodology and technology. *Environmental Science and Technology*, *40*(17), 5181–5192. https://doi.org/10.1021/es0605016

Logan, B. E., & Regan, J. M. (2006). Microbial fuel cells-challenges and applications. *Environmental Science and Technology*, *40*(17), 5172–5180. https://doi.org/10.1021/es0627592

Monroy, I., Guevara-López, E., & Buitrón, G. (2018). Biohydrogen production by batch indoor and outdoor photo-fermentation with an immobilized consortium: A process model with neural networks. *Biochemical Engineering Journal*, *135*, 1–10. https://doi.org/10.1016/j.bej.2018.01.026

Mowbray, M., Savage, T., Wu, C., Song, Z., Cho, B. A., Del Rio-Chanona, E. A., & Zhang, D. (2021). Machine learning for biochemical engineering: A review. *Biochemical Engineering Journal*, *172*, 108054. https://doi.org/10.1016/j.bej.2021.108054

Nazari, A. (2012). Prediction performance of PEM fuel cells by gene expression programming. *International Journal of Hydrogen Energy*, *37*(24), 18972–18980. https://doi.org/10.1016/j.ijhydene.2012.08.101

Ojha, P. C., Satpathy, S. S., Ojha, A. K., Sukla, L. B., & Pradhan, D. (2022). Overcoming challenges due to enhanced biomedical waste generation during COVID-19 pandemic. *Science of the Total Environment*, *832*, 155072. https://doi.org/10.1016/j.scitotenv.2022.155072

Ojha, R., Dash, J., Satpathy, S. S., Ojha, P. C., & Pradhan, D. (2025). A brief review on factors affecting the performance of microbial fuel cell and integration of artificial intelligence. *Discover Sustainability*, *6*(1), 702. https://doi.org/10.1007/s43621-025-01619-6

Ojha, R., & Pradhan, D. (2025). The potential of microbial fuel cell for converting waste to energy: An overview. *Sustainable Chemistry for the Environment*, *9*, 100196. https://doi.org/10.1016/j.scenv.2024.100196

Pandya, R. S., Kaur, T., Bhattacharya, R., Bose, D., & Saraf, D. (2024). Harnessing microorganisms for bioenergy with microbial fuel cells: Powering the future. *Water-Energy Nexus*, *7*, 1–12. https://doi.org/10.1016/j.wen.2023.11.004

Prathiba, S., Kumar, P. S., & Rangasamy, G. (2024). Recent advancements on the development of microbial fuel cells: Anode modification and scale-up challenges in upgrading anode electrode. *International Journal of Hydrogen Energy*, *107*, 123–134. https://doi.org/10.1016/j.ijhydene.2024.02.144

Rai, R., Tiwari, M. K., Ivanov, D., & Dolgui, A. (2021). *Machine learning in manufacturing and industry 4.0 applications* (Vol. 59). Taylor & Francis.

Recio-Garrido, D., Perrier, M., & Tartakovsky, B. (2016). Modeling, optimization and control of bioelectrochemical systems. *Chemical Engineering Journal*, *289*, 180–190. https://doi.org/10.1016/j.cej.2015.11.112

Rezk, H., Olabi, A., Abdelkareem, M. A., & Sayed, E. T. (2023). Artificial intelligence as a novel tool for enhancing the performance of urine fed microbial fuel cell as an emerging approach for simultaneous power generation and wastewater treatment. *Journal of the Taiwan Institute of Chemical Engineers*, *148*, 104726. https://doi.org/10.1016/j.jtice.2023.104726

Satpathy, S. S., Ojha, P. C., Ojha, R., Dash, J., & Pradhan, D. (2025). Recent modifications of anode materials and performance evaluation of microbial fuel cells: A brief review. *Journal of Energy Engineering*, *151*(2), 03125001. https://doi.org/10.1061/JLEED9.EYENG-5732

Satpathy, S. S., Ojha, P. C., & Pradhan, D. (2022). Development of dairy wastewater treatment for valuable applications. In *International conference on water technologies* (pp. 73–95). Springer Nature Singapore.

Sayed, E. T., Rezk, H., Abdelkareem, M. A., & Olabi, A. (2024). Artificial neural network based modelling and optimization of microalgae microbial fuel cell. *International Journal of Hydrogen Energy*, *52*, 1015–1025. https://doi.org/10.1016/j.ijhydene.2022.12.081

Sevda, S., Garlapati, V. K., & Sreekrishnan, T. (2023). Role of electrode and proton exchange membrane configurations on microbial fuel cell performance toward bioelectricity generation integrated wastewater treatment. *Journal of Environmental Science and Health, Part A*, *58*(1), 13–23. https://doi.org/10.1080/10934529.2023.2168998

Shabani, F., Philamore, H., & Matsuno, F. (2021). An energy-autonomous chemical oxygen demand sensor using a microbial fuel cell and embedded machine learning. *IEEE Access*, *9*, 108689–108701. https://doi.org/10.1109/ACCESS.2021.3101496

Ta, Q. T. H., Nguyen, P. K. T., & Nguyen, P. K. T. (2022). Artificial intelligence-based modeling and optimization of microbial electrolysis cell-assisted anaerobic digestion fed with alkaline-pretreated waste-activated sludge. *Biochemical Engineering Journal*, *187*, 108670. https://doi.org/10.1016/j.bej.2022.108670

Tardast, A., Rahimnejad, M., Najafpour, G., Pirzade, K., & Mokhtarian, N. (2012). Prediction of bioelectricity production by neural network. *Journal of Biotechnology and Pharmaceutical Research*, *3*(3), 62–68.

Vichard, L., Harel, F., Ravey, A., Venet, P., & Hissel, D. (2020). Degradation prediction of PEM fuel cell based on artificial intelligence. *International Journal of Hydrogen Energy*, *45*(29), 14953–14963. https://doi.org/10.1016/j.ijhydene.2020.03.209

Wang, J., Ding, R., Cao, F., Li, J., Dong, H., Shi, T., Xing, L., & Liu, J. (2022). Comparison of state-of-the-art machine learning algorithms and data-driven optimization methods for mitigating nitrogen crossover in PEM fuel cells. *Chemical Engineering Journal*, *442*, 136064. https://doi.org/10.1016/j.cej.2022.136064

Xu, B., Sun, Q.-J., Lan, J. C.-W., Chang, M.-H., Hsueh, C.-C., & Chen, B.-Y. (2019). Deciphering electron-shuttling characteristics of microalgal metabolites upon bioelectricity-generating community in microbial fuel cells. *Biochemical Engineering Journal*, *144*, 148–156. https://doi.org/10.1016/j.bej.2019.01.018

Yaman, O. U., & Çalık, P. (2023). MachineTFBS: Motif-based method to predict transcription factor binding sites with first-best models from machine learning library. *Biochemical Engineering Journal*, *198*, 108990. https://doi.org/10.1016/j.bej.2023.108990

Yewale, A., Methekar, R., & Agrawal, S. (2020). Multiple model-based control of multi variable continuous microbial fuel cell (CMFC) using machine learning approaches. *Computers & Chemical Engineering*, *140*, 106884. https://doi.org/10.1016/j.compchemeng.2020.106884

You, J., Yu, J., Zhang, S., Chen, J., & Chen, D. (2023). Performance and mechanism of innovative two-phase partitioning microbial fuel cell for effective propanethiol treatment. *Chemical Engineering Journal*, *453*, 139731. https://doi.org/10.1016/j.cej.2022.139731

Zhou, N., Price, L., Yande, D., Creyts, J., Khanna, N., Fridley, D., Lu, H., Feng, W., Liu, X., Hasanbeigi, A., Tian, Z., Yang, H., Bai, Q., Zhu, Y., Xiong, H., Zhang, J., Chrisman, K., Agenbroad, J.Ke, Y. . . . Yee, C. (2019). A roadmap for China to peak carbon dioxide emissions and achieve a 20% share of non-fossil fuels in primary energy by 2030. *Applied Energy*, *239*, 793–819. https://doi.org/10.1016/j.apenergy.2019.01.154